# PHYSICS-INFORMED MACHINE LEARNING-BASED CLOUD MICROPHYSICS PARAMETERIZATION FOR EARTH SYSTEM MODELS

**Ellen Sarauer**
Deutsches Zentrum für Luft- und Raumfahrt
Institut für Physik der Atmosphäre
Oberpfaffenhofen
Germany
ellen.sarauer@dlr.de

**Mierk Schwabe**
Deutsches Zentrum für Luft- und Raumfahrt
Institut für Physik der Atmosphäre
Oberpfaffenhofen
Germany

**Philipp Weiss**
Atmospheric, Oceanic and Planetary Physics
Department of Physics
University of Oxford
UK

**Axel Lauer**
Deutsches Zentrum für Luft- und Raumfahrt
Institut für Physik der Atmosphäre
Oberpfaffenhofen
Germany

**Philip Stier**
Atmospheric, Oceanic and Planetary Physics
Department of Physics
University of Oxford
UK

**Veronika Eyring**
Deutsches Zentrum für Luft- und Raumfahrt
Institut für Physik der Atmosphäre
Oberpfaffenhofen
University of Bremen
Bremen
Germany

## ABSTRACT

In this study, we develop a physics-informed machine learning (ML)-based cloud microphysics parameterization for the ICON model. By training the ML parameterization on high-resolution simulation data, we aim to improve Earth System Models (ESMs) in comparison to traditional parameterization schemes. We investigate the usage of a multilayer perceptron (MLP) with feature engineering and physics-constraints, and use explainability techniques to understand the relationship between input features and model output. Our novel approach yields promising results, with the physics-informed ML-based cloud microphysics parameterization achieving an $R^2$ score up to 0.777 for an individual feature. Additionally, we demonstrate a notable improvement in the overall performance in comparison to a baseline MLP, increasing its average $R^2$ score from 0.290 to 0.613 across all variables. This approach to improve the representation of cloud microphysics in ESMs promises to enhance climate projections, contributing to a better understanding of climate change.

## 1 INTRODUCTION

Machine learning (ML) made great strides in enhancing Earth System Models (ESMs) by replacing traditional parameterizations that are based on empirical and physical understanding and represent the statistical effect of a given process at the grid scale of the climate model (Rasp et al., 2018; Reichstein et al., 2019; Eyring et al., 2023b). For this, typically ML models are trained on high-resolution climate simulations or observations and then coupled to the coarse climate model, potentially eliminating long-standing biases in ESMs (Gentine et al., 2021; Grundner et al., 2022;

Eyring et al., 2023a). However, in the literature, the cloud microphysics parameterization has only been emulated on the same resolution as the simulation data (Gettelman et al., 2021; Han et al., 2020; Perkins et al., 2023). Therefore, this study presents a novel approach for learning the cloud microphysics parameterization by incorporating higher resolution dynamics into the lower resolution ESM. This will be especially beneficial when parameterizing cloud convection together with cloud microphysics in future studies. The parameterization of cloud microphysics is central in traditional ESMs, working closely coupled to the convection scheme in order to model the behavior of clouds. It calculates the formation, growth and removal of cloud liquid water particles and captures phase changes. Additionally, cloud microphysics processes impact the lifetime of clouds, the water vapor distribution outside of clouds, the fluxes of water and radiation through the atmosphere, and latent heating. We aim to enhance the representation of subgrid-scale cloud microphysics within the coarse-scale Icosahedral Non-hydrostatic modeling framework (ICON) (Zängl et al., 2014; Giorgetta et al., 2018), which traditionally employs the single moment microphysical scheme (Lohmann & Roeckner, 1996). This scheme focuses on prognostic equations for the mass mixing ratios (MMRs) of water vapor, cloud liquid water, cloud ice, and rain. In order to improve upon this baseline, we propose the development of an ML-based parameterization that is trained on ICON simulation data that uses the more complex graupel scheme (Rutledge & Hobbs, 1984; Baldauf et al., 2011). The graupel scheme not only calculates the MMR of snow and graupel but also provides precipitation rates for rain, snow, and graupel. Moreover, the use of high-resolution simulation data allows us to incorporate the statistical effects of higher-resolved dynamics into the ML model. This holds the potential to further improve the cloud microphysics parameterization and enhance the accuracy of ESMs.

## 2 METHODOLOGY

### 2.1 UNDERLYING DATASET

We generate high-resolution data through a simulation setup utilizing the atmospheric component of ICON Sapphire (Hohenegger et al., 2023; NextGems, 2024) with a horizontal resolution of roughly 5 km. An illustration of the simulation is given in the Appendix A, Figure 3. The model time step for cloud microphysics is set to 40 seconds. To keep the data volume manageable, we store data every three simulated hours, namely, the mean over that time period of all input and output parameters used in the ML parameterization (see below). We run the simulation for 30 days from 20 January 2020 and discard the first ten days as spin-up period. We use ERA5 boundary conditions from Hersbach et al. (2020) to initialize the model with historical weather data, ozone concentrations, aerosol concentrations, ocean properties like the sea surface temperature and sea salt concentration, and land properties. Subsequently, we proceed to a coarse-graining technique where we compute the mean of the variables using a weighting system based on the grid cell size, adopting the same methodology as Grundner et al. (2022), mapping the data to a coarser ICON grid with a horizontal resolution of 80 km. We consider a cell-based approach and preselect for grid cells that contain a sufficient amount of cloud MMR (cloud liquid water $m_{\mathrm{qc}}$, cloud ice $m_{\mathrm{qi}}$) or precipitation MMR (rain $m_{\mathrm{qr}}$, snow $m_{\mathrm{qs}}$, graupel $m_{\mathrm{qg}}$) defined as follows

$$(m_{\mathrm{qc}} + m_{\mathrm{qi}}) \geq 10^{-5}\,\mathrm{kg}\cdot\mathrm{kg}^{-1}, \quad (m_{\mathrm{r}} + m_{\mathrm{s}} + m_{\mathrm{g}}) \geq 10^{-7}\,\mathrm{kg}\cdot\mathrm{kg}^{-1}. \tag{1}$$

The coarse-graining and preselection strategy results in a total data set size of approximately $6.4$ million samples, which we randomly split into training, validation and testing sets. We scale the data with respect to the standard deviation and the mean of the training set.

### 2.2 MACHINE LEARNING MODEL

As discussed in de Burgh-Day & Leeuwenburg (2023), incorporating domain knowledge into ML parameterizations increases the performance. Figure 1 shows an overview of the ML parameterization developed in this work. Since the goal is to run the ML model online in an ICON simulation run, we prioritize a simpler model architecture (shown in blue in the figure) and focus on implementing additional meaningful input features, introducing constraints to avoid unphysical negative MMRs, and explain the model's behavior with explainability methods. The training of the base multilayer perceptron (MLP) model is structured as follows: 27 input nodes for the microphysical input parameters, three hidden layers with 256 nodes each using the ReLu

activation (Agarap, 2019), 7 output nodes using linear activation. For the used set of input and output parameters and their description the reader is referred to the Appendix A, Table 2. We train the model over 100 epochs and optimize the model's hyperparameters with the Keras tuner (O'Malley et al., 2019). Feature engineering provides a methodology to incorporate additional physical information into the ML parameterization model (Zheng et al., 2021). Since the Graupel scheme calculates the phase transition from different microphysical tracers, we introduce the relative difference in MMRs between the aggregate states of water as an additional model input. The relative difference $\Delta m_{q1,q2}$ for MMRs $m$ of the tracers $q_1$ and $q_2$ is defined as follows:

$$\Delta m_{q_1,q_2} = \frac{m_{q_1} - m_{q_2}}{m_{q_2}}, \quad \text{if } m_{q_2} > 0, \quad \text{else } \Delta m_{q_1,q_2} = 0. \tag{2}$$

During the preselection procedure of our simulated dataset we find that the classical parameterization produces negative masses, or tendencies that lead to negative masses after the application of the classical parameterization in 4% of the samples in the preselected dataset. When these effects occur in the classical parameterization, the ICON model sets the negative masses to zero and recalculates the tendencies. To incorporate this correction into our model, we apply the method of physics constraining for negative masses following the approach of Harder et al. (2022). We modify the weights of the output layer during the optimization of the MLP, constraining all tendencies $\Delta q$ not fulfilling the condition

$$m_{q,t1} = m_{q,t0} + \Delta t \cdot \Delta q \geq 0. \tag{3}$$

Here, $m_{q,t1}$ is the MMR after the application of the parameterization, and $m_{q,t0}$ the MMR before the application of the parameterization. The tendency $\Delta q$ represents the rate of change of the MMR per internal model time step $\Delta t$ in the ICON simulation, which is 40 s in this study. Finally, for the purpose of explainability, the input feature importance ranking performed in this study is computed via the SHAP package (Lundberg & Lee, 2017). This package follows the game theory approach of the calculation of Shapley values.

## 3 Results

Our study evaluates the performance of the physics-informed MLP algorithm with feature engineering (blue, yellow and green model in Figure 1) on the coarse-grained ICON simulation test dataset in comparison with the physics-informed MLP model without feature-engineered input variables (blue and green model in Figure 1). By hyperparameter tuning with Keras tuner, we identify the physics-informed ML algorithm that best captures the characteristics of the coarse-grained high-resolution simulation data and the additional input features. Even though the cloud microphysics parameterization is a complex problem to tackle (cf. Appendix A, Figure 4), we are able to reach a goodness of fit of 0.613 $R^2$ score averaged over all output features, with achieving the best regression output for the cloud liquid water MMR (0.777 $R^2$ score). For the specific goodness of fit for the individual output features are presented in Table 2. The goodness of fit for the tendencies of temperature and cloud properties (water vapor, cloud liquid water and cloud ice) are better compared to the tendencies for precipitation (rain, snow, graupel). This may be due to a lack of events with high precipitation MMR in the training dataset. With the introduction of additional input features, we are able to improve the model's performance from

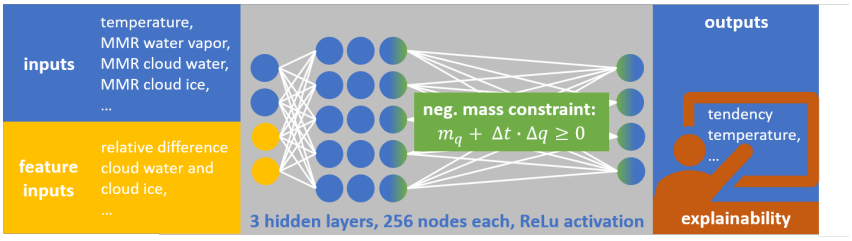


Figure 1: Overview of the presented ML parameterization. The baseline MLP model is shown (blue) with additional input features obtained via feature engineering (yellow), negative mass constraining (green) and explainability (red).

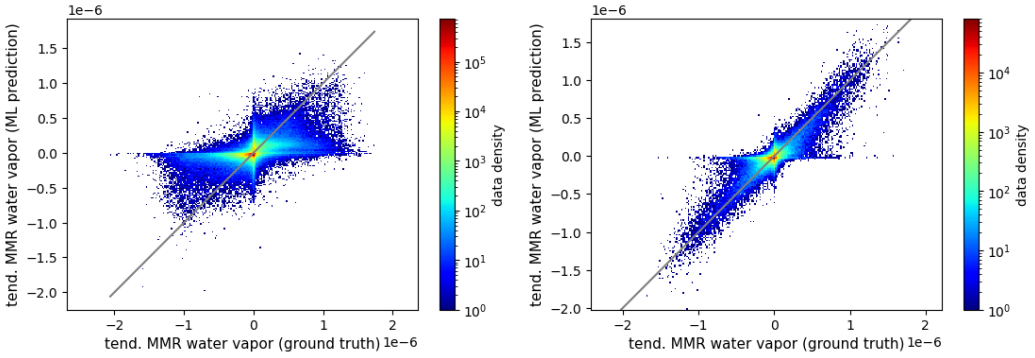


Figure 2: ML predictions vs. ground truth of water vapor MMR tendencies without (left) and with (right) additional input features. The colors illustrate the density of the data on a logarithmic scale.

0.290 to 0.613 $R^2$ score. As an example, the tendency of the MMR of water vapor is examined in Figure 2, showcasing the outcomes of the feature engineering technique. In the panels, the ML parameterization predictions of the tendencies are shown as function of the training data for the MLP trained without (left) resp. with (right) the feature-engineered input. Both figures indicate that the ML parameterization overestimates tendencies that are zero in the classical parameterization or the ML prediction. This could be due to an over-representation of microphysical tracers with values very close to zero in their distributions. Moreover, the MLP trained without feature-engineered input variables exhibits a more extensive spread of data compared to that incorporating the additional input variables. We see an enhancement of the model's performance through feature engineering. However, by training the baseline MLP on a more balanced training data set, we can anticipate the model to independently capture these features. The comparison between model prediction and test dataset (ground truth) for the other variables can be found in Appendix A, Figure 5. In contrast to feature engineering, constraining unphysical values in the training dataset as described above does not have an impact on the overall performance of the ML parameterization. Nevertheless, we expect the constrained ML parameterization to lead to an improved and more stable simulation when coupled to the climate model in future work. Furthermore, we employ explainability techniques to gain a better understanding of the relationships between different input features and the resulting model output, i.e., microphysical tendencies. Detected by the Shapley value calculation, we observe a strong correlation between the microphysical tendencies and both air pressure and temperature. This is due to clouds and precipitation occuring more often at certain height levels and the direct influence of temperature on phase transitions. Moreover, the vertical velocity and meridional wind also play a significant role in determining the microphysical properties. This could stem from the fact that convective clouds are coupled to the strong vertical updraft, and that the overall dynamics of the atmosphere are strongly influenced by the wind. We will elaborate on this aspect in future work when

Table 1: Goodness of fit measures for the regression output in the ML parameterization without additional input features (base) compared with additional input features (marked bold). The table shows for each output variable: arithmetic average (mean) and standard deviation ($\sigma$), root mean squared error (RMSE), and squared pearson correlation ($R^2$).

| OUTPUT | MEAN | $\sigma$ | RMSE (base) | RMSE | $R^2$ (base) | $R^2$ |
|---|---|---|---|---|---|---|
| tend_ta_mig | $3.87{\cdot}10^{-5}$ | $2.31{\cdot}10^{-4}$ | $1.83{\cdot}10^{-4}$ | $\mathbf{1.21{\cdot}10^{-4}}$ | 0.370 | **0.726** |
| tend_qv_mig | $1.77{\cdot}10^{-8}$ | $9.91{\cdot}10^{-8}$ | $7.88{\cdot}10^{-8}$ | $\mathbf{5.14{\cdot}10^{-8}}$ | 0.367 | **0.731** |
| tend_qc_mig | $8.51{\cdot}10^{-10}$ | $8.92{\cdot}10^{-8}$ | $4.21{\cdot}10^{-8}$ | $\mathbf{5.20{\cdot}10^{-8}}$ | 0.412 | **0.777** |
| tend_qi_mig | $2.71{\cdot}10^{-10}$ | $2.92{\cdot}10^{-9}$ | $2.37{\cdot}10^{-9}$ | $\mathbf{1.63{\cdot}10^{-9}}$ | 0.337 | **0.687** |
| tend_qr_mig | $1.13{\cdot}10^{-9}$ | $1.71{\cdot}10^{-8}$ | $1.54{\cdot}10^{-8}$ | $\mathbf{1.22{\cdot}10^{-8}}$ | 0.188 | **0.492** |
| tend_qs_mig | $5.46{\cdot}10^{-10}$ | $8.91{\cdot}10^{-9}$ | $8.33{\cdot}10^{-9}$ | $\mathbf{6.97{\cdot}10^{-9}}$ | 0.126 | **0.388** |
| tend_qg_mig | $5.02{\cdot}10^{-10}$ | $2.11{\cdot}10^{-8}$ | $1.86{\cdot}10^{-8}$ | $\mathbf{1.51{\cdot}10^{-8}}$ | 0.226 | **0.493** |

parameterizing microphysics together with convection. Additionally, the feature importance for the variables that describe the relative difference between the tracers is larger than that of the MMRs themselves. This implies that the additional input features derived with the feature engineering method are a good choice.

## 4 DISCUSSION

In this study, we conduct a 5 km-scale simulation with the atmospheric component of the Earth System Model ICON to produce a dataset that contains inputs and outputs of the existing cloud microphysics parameterization. We coarse-grain the data to 80 km resolution, train an MLP model by including physical information through feature engineering, and ensure meaningful outputs of the model by incorporating the physical constraint of preventing negative masses. By ranking the feature importance, we are able to find the most important input features for the ML parameterization. The physics-informed ML-based cloud microphysics parameterization achieves a goodness of fit of up to 0.777 $R^2$ score for one individual feature. We improve the baseline MLP model's performance from 0.290 $R^2$ score to 0.613 $R^2$ score averaged over all variables. Nevertheless, the model performance can be further improved by generating a more balanced dataset, e.g. conducting multiple shorter simulations at different times of the year. Moreover, the full benefits of this approach will only become apparent when implementing this ML-based microphysics parameterization in a global climate model. Overall, our study presents a novel approach to parameterize cloud microphysical processes by introducing small-scale dynamical processes from high resolution simulations. The findings of this research provide a foundation for a future cloud microphysics and convection parameterization, reducing the uncertainties of clouds in climate simulations with current models. With our work, we aim to improve the accuracy and reliability of climate projections, contributing to a better understanding of climate change and its implications.

### ACKNOWLEDGMENTS

This project was made possible by the DLR Quantum Computing Initiative and the Federal Ministry for Economic Affairs and Climate Action and by the European Research Council (ERC) Synergy Grant "Understanding and Modelling the Earth System with Machine Learning (USMILE)" under the Horizon 2020 research and innovation programme (Grant agreement No. 855187). Philip Stier and Philipp Weiss acknowledge funding from the Horizon 2020 projects nextGEMS under grant agreement number 101003470 and FORCeS under grant agreement number 821205. This work used resources of the Deutsches Klimarechenzentrum (DKRZ) granted by its Scientific Steering Committee (WLA) under project ID bd1179. The authors gratefully acknowledge the Earth System Modelling Project (ESM) for funding this work by providing computing time on the ESM partition of the supercomputer JUWELS Jülich Supercomputing Centre (2021) at the Jülich Supercomputing Centre (JSC).

## REFERENCES

A. F. Agarap. Deep learning using rectified linear units (relu), 2019.

M. Baldauf, A. Seifert, J. Förstner, D. Majewski, M. Raschendorfer, and T. Reinhardt. Operational convective-scale numerical weather prediction with the cosmo model: Description and sensitivities. *Monthly Weather Review*, 139(12):3887 – 3905, 2011. doi: 10.1175/MWR-D-10-05013.1.

C. de Burgh-Day and T. Leeuwenburg. Machine learning for numerical weather and climate modelling: a review. *Geoscientific Model Development*, 16:6433–6477, 11 2023. doi: 10.5194/gmd-16-6433-2023.

V. Eyring, W.D. Collins, P. Gentine, E.A. Barnes, M. Barreiro, T. Beucler, M. Bocquet, C.S. Bretherton, H.M. Christensen, D.J. Gagne, D. Hall, D. Hammerling, S. Hoyer, F. Iglesias-Suarez, I. Lopez-Gomez, M.C. McGraw, G.A. Meehl, M.J. Molina, C. Monteleoni, J. Mueller, M.S. Pritchard, D. Rolnick, J. Runge, P. Stier, O. Watt-Meyer, K. Weigel, R. Yu, and L. Zanna. Pushing the frontiers in climate modelingand analysis with machine learning. *Nature Climate Change*, submitted, 2023a.

V. Eyring, P. Gentine, G. Camps-Valls, D. M. Lawrence, and M. Reichstein. Next-generation earth system modeling to address urgent mitigation and adaptation needs. *Nature Geoscience*, submitted, 2023b.

P. Gentine, Ve. Eyring, and T. Beucler. *Deep Learning for the Parametrization of Subgrid Processes in Climate Models*, pp. 307–314. John Wiley & Sons, Ltd, 2021. ISBN 978-1-119-64618-1. doi: https://doi.org/10.1002/9781119646181.ch21.

A. Gettelman, D. J. Gagne, C.-C. Chen, M. W. Christensen, Z. J. Lebo, H. Morrison, and G. Gantos. Machine learning the warm rain process. *Journal of Advances in Modeling Earth Systems*, 13(2): e2020MS002268, 2021. doi: https://doi.org/10.1029/2020MS002268.

M. A. Giorgetta, R. Brokopf, T. Crueger, M. Esch, S. Fiedler, J. Helmert, C. Hohenegger, L. Kornblueh, M. Köhler, E. Manzini, T. Mauritsen, C. Nam, T. Raddatz, S. Rast, D. Reinert, M. Sakradzija, H. Schmidt, R. Schneck, R. Schnur, L. Silvers, H. Wan, G. Zängl, and B. Stevens. Icon-a, the atmosphere component of the icon earth system model: I. model description. *Journal of Advances in Modeling Earth Systems*, 10(7):1613–1637, 2018. doi: https://doi.org/10.1029/2017MS001242.

A. Grundner, T. Beucler, P. Gentine, F. Iglesias-Suarez, M. A. Giorgetta, and V. Eyring. Deep learning based cloud cover parameterization for icon. *Journal of Advances in Modeling Earth Systems*, 14(12):e2021MS002959, 2022. doi: https://doi.org/10.1029/2021MS002959.

Y. Han, G. J. Zhang, X. Huang, and Y. Wang. A moist physics parameterization based on deep learning. *Journal of Advances in Modeling Earth Systems*, 12(9):e2020MS002076, 2020. doi: https://doi.org/10.1029/2020MS002076.

P. Harder, D. Watson-Parris, P. Stier, D. Strassel, N. R. Gauger, and J. Keuper. Physics-informed learning of aerosol microphysics. *Environmental Data Science*, 1:e20, 2022. doi: 10.1017/eds.2022.22.

H. Hersbach, B. Bell, P. Berrisford, S. Hirahara, A. Horányi, J. Muñoz-Sabater, J. Nicolas, C. Peubey, R. Radu, D. Schepers, A. Simmons, C. Soci, S. Abdalla, X. Abellan, G. Balsamo, P. Bechtold, G. Biavati, J. Bidlot, M. Bonavita, G. De Chiara, P. Dahlgren, D. Dee, M. Diamantakis, R. Dragani, J. Flemming, R. Forbes, M. Fuentes, A. Geer, L. Haimberger, S. Healy, R. J. Hogan, E. Hólm, M. Janisková, S. Keeley, P. Laloyaux, P. Lopez, C. Lupu, G. Radnoti, P. de Rosnay, I. Rozum, F. Vamborg, S. Villaume, and J. Thépaut. The ERA5 global reanalysis. *Quarterly Journal of the Royal Meteorological Society*, 146(730):1999–2049, 2020. ISSN 1477-870X. doi: 10.1002/qj.3803.

C. Hohenegger, P. Korn, L. Linardakis, R. Redler, R. Schnur, P. Adamidis, J. Bao, S. Bastin, M. Behravesh, M. Bergemann, J. Biercamp, H. Bockelmann, R. Brokopf, N. Brüggemann, L. Casaroli, F. Chegini, G. Datseris, M. Esch, G. George, M. Giorgetta, O. Gutjahr, H. Haak, M. Hanke, T. Ilyina, T. Jahns, J. Jungclaus, M. Kern, D. Klocke, L. Kluft, T. Kölling, L. Kornblueh, S. Kosukhin, C. Kroll, J. Lee, T. Mauritsen, C. Mehlmann, T. Mieslinger, A. K. Naumann, L. Paccini, A. Peinado, D. S. Praturi, D. Putrasahan, S. Rast, T. Riddick, N. Roeber, H. Schmidt, U. Schulzweida, F. Schütte, H. Segura, R. Shevchenko, V. Singh, M. Specht, C. C. Stephan, J.-S. von Storch, R. Vogel, C. Wengel, M. Winkler, F. Ziemen, J. Marotzke, and B. Stevens. Icon-sapphire: simulating the components of the earth system and their interactions at kilometer and subkilometer scales. *Geoscientific Model Development*, 16(2):779–811, 2023. doi: 10.5194/gmd-16-779-2023.

Jülich Supercomputing Centre. JUWELS Cluster and Booster: Exascale Pathfinder with Modular Supercomputing Architecture at Juelich Supercomputing Centre. *Journal of large-scale research facilities*, 7(A138), 2021. doi: 10.17815/jlsrf-7-183. URL `http://dx.doi.org/10.17815/jlsrf-7-183`.

U. Lohmann and E. Roeckner. Design and performance of a new cloud microphysics scheme developed for the echam general circulation model. *Climate Dynamics*, 12:557–572, 1996.

S. M. Lundberg and S. Lee. A unified approach to interpreting model predictions. In I. Guyon, U. V. Luxburg, S. Bengio, H. Wallach, R. Fergus, S. Vishwanathan, and R. Garnett (eds.), *Advances in Neural Information Processing Systems 30*, pp. 4765–4774. Curran Associates, Inc., 2017.

2021 NextGems. Next generation earth modelling systems. https://cordis.europa.eu/project/id/101003470, 2024. Accessed 22 January 2024.

T. O'Malley, E. Bursztein, J. Long, F. Chollet, H. Jin, L. Invernizzi, et al. Kerastuner, 2019. https://github.com/keras-team/keras-tuner, 2019. Accessed 15 December 2023.

W. A. Perkins, N. D. Brenowitz, C. S. Bretherton, and J. M. Nugent. *Emulation of cloud microphysics in a climate model*. June 2023. doi: 10.22541/essoar.168614667.71811888/v1.

S. Rasp, M. S. Pritchard, and P. Gentine. Deep learning to represent sub-grid processes in climate models. *Proceedings of the National Academy of Sciences*, 115(39):9684–9689, September 2018. ISSN 0027-8424, 1091-6490. doi: 10.1073/pnas.1810286115. arXiv:1806.04731 [physics, stat].

M. Reichstein, G. Camps-Valls, B. Stevens, M. Jung, J. Denzler, N. Carvalhais, and Prabhat. Deep learning and process understanding for data-driven earth system science. *Nature*, 566(7743): 195–204, February 2019. ISSN 1476-4687. doi: 10.1038/s41586-019-0912-1.

S. A. Rutledge and P. V. Hobbs. The mesoscale and microscale structure and organization of clouds and precipitation in midlatitude cyclones. xii: A diagnostic modeling study of precipitation development in narrow cold-frontal rainbands. *Journal of Atmospheric Sciences*, 41(20):2949 – 2972, 1984. doi: 10.1175/1520-0469(1984)041⟨2949:TMAMSA⟩2.0.CO;2.

NASA visible earth. NASA visible earth. https://visibleearth.nasa.gov/, 2024. Accessed 22 January 2024.

G. Zängl, D. Reinert, P. Rípodas, and M. Baldauf. The ICON (ICOsahedral Non-hydrostatic) modelling framework of DWD and MPI-M: Description of the non-hydrostatic dynamical core. *Quarterly Journal of the Royal Meteorological Society*, 141(687):563–579, June 2014. doi: 10.1002/qj.2378.

L. Zheng, R. Lin, X. Wang, and W. Chen. The development and application of machine learning in atmospheric environment studies. *Remote Sensing*, 13(23), 2021. ISSN 2072-4292. doi: 10.3390/rs13234839.

# A Appendix

### Additional figures

Figure 3 illustrates the underlying simulated dataset of this work. This figure shows the microphysical MMRs. These parameters are important input features for the ML parameterization developed in this work.

Figure 4 shows the correlation between the considered input and output variables. It can be seen that the input and output show low correlation. Therefore, one needs to include domain knowledge, e.g., physics-constraints and feature engineering into the model.

Figure 5 illustrates the goodness of fit results individually for all the output variables, i.e., the microphysical tendencies.

### Additional tables

Table 2 lists the variables considered in this work. The variables added in the feature engineering approach are marked as 'Feature Input'. The bold marked inputs are the ten most important input features for the physics-informed MLP.

### Computing Resources

We are only able to run the simulation for this short amount of time because of the substantial computing resources necessary for running such a simulation (12k node hours for 30 days simulation) and storing such a large volume of data (25 TB for the 20 days of high-resolution data when reduced to 3-hourly output).

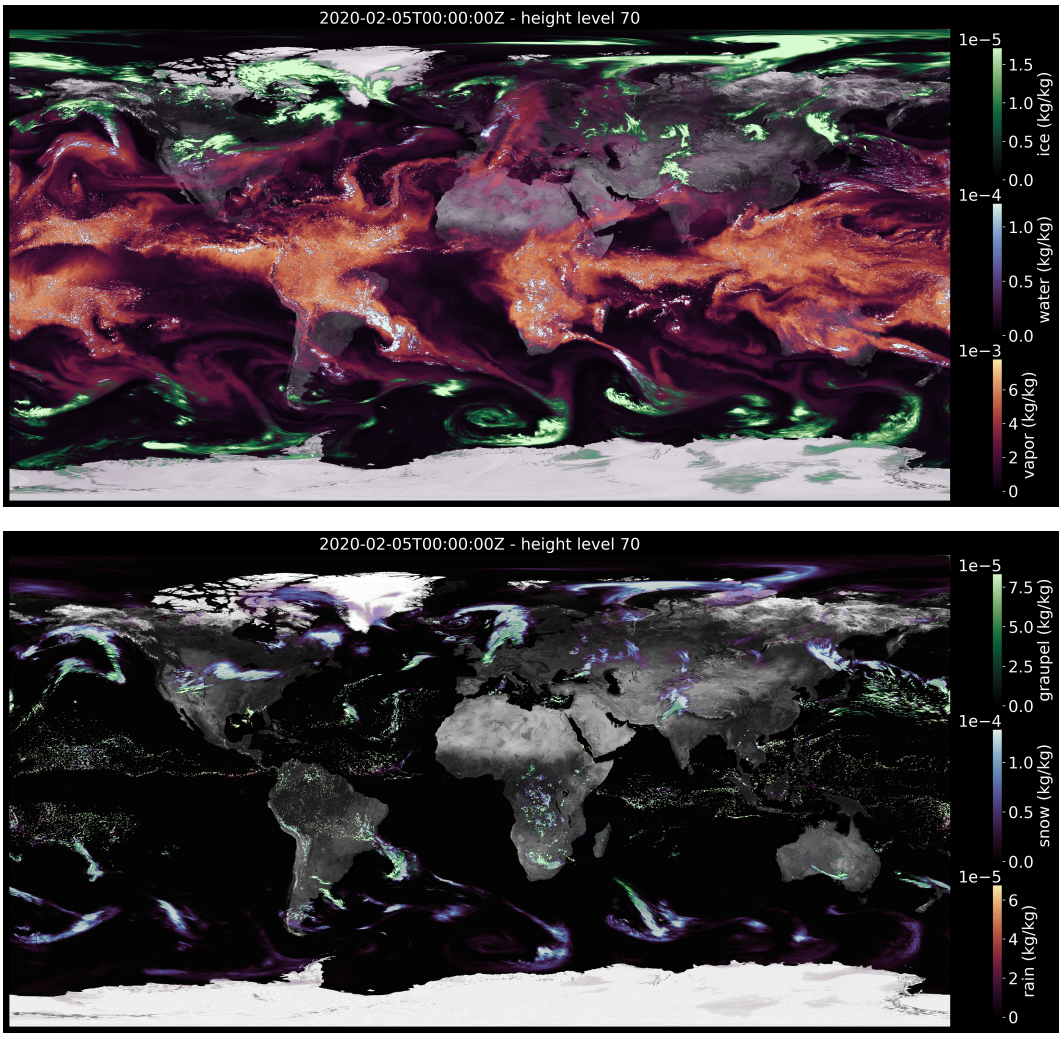


Figure 3: Map of MMRs obtained from the simulation on model level 70 corresponding to a height of about 3 kilometers. The upper figure shows water vapor (red), cloud liquid water (blue) and cloud ice (green). The lower figure shows rain (red), snow (blue) and graupel (green). Earth illustration from visible earth (2024).

Table 2: Overview of all considered input and output features of the MLP model. The inputs marked as 'Feature input' are the additional features that stem from the feature engineering approach. The inputs marked in bold text are the ten most important input features determined by Shapley values.

| TYPE | SHORT NAME | DESCRIPTION | UNIT |
|---|---|---|---|
| **Input** | **pf_mig** | **air pressure** | **Pa** |
| **Input** | **ta_mig** | **temperature** | **T** |
| **Input** | **omega** | **vertical velocity** | **m/s** |
| Input | ua_mig | zonal wind | m/s |
| **Input** | **va_mig** | **meridional wind** | **m/s** |
| Input | qv_mig | cloud vapor MMR | kg/kg |
| Input | qc_mig | cloud liquid water MMR | kg/kg |
| Input | qi_mig | cloud ice MMR | kg/kg |
| Input | qs_mig | snow MMR | kg/kg |
| Input | qr_mig | rain MMR | kg/kg |
| Input | qg_mig | graupel MMR | kg/kg |
| Feature Input | diff_qv_qc | rel. diff. water vapor / cloud liquid water MMRs | 1 |
| Feature Input | diff_qv_qr | rel. diff. water vapor / rain MMRs | 1 |
| Feature Input | diff_qi_qv | rel. diff. cloud ice / water vapor MMRs | 1 |
| Feature Input | diff_qs_qv | rel. diff. snow / water vapor MMRs | 1 |
| Feature Input | diff_qv_qg | rel. diff. water vapor / graupel MMRs | 1 |
| **Feature Input** | **diff_qc_qi** | **rel. diff. cloud liquid water / cloud ice MMRs** | **1** |
| Feature Input | diff_qc_qr | rel. diff. cloud liquid water / rain MMRs | 1 |
| Feature Input | diff_qs_qc | rel. diff. snow / cloud liquid water MMRs | 1 |
| **Feature Input** | **diff_qg_qc** | **rel. diff. graupel / cloud liquid water MMRs** | **1** |
| **Feature Input** | **diff_qr_qs** | **rel. diff. rain / snow MMRs** | **1** |
| **Feature Input** | **diff_qi_qr** | **rel. diff. cloud ice / rain MMRs** | **1** |
| Feature Input | diff_qr_qg | rel. diff. rain / graupel MMRs | 1 |
| Feature Input | diff_qi_qs | rel. diff. cloud ice / snow MMRs | 1 |
| **Feature Input** | **diff_qg_qi** | **rel. diff. graupel / cloud ice MMRs** | **1** |
| **Feature Input** | **diff_qs_qg** | **rel. diff. snow / graupel MMRs** | **1** |
| Output | tend_ta_mig | tendency of temperature | T/s |
| Output | tend_qv_mig | tendency of cloud vapor MMR | kg/(kg·s) |
| Output | tend_qc_mig | tendency of cloud liquid water MMR | kg/(kg·s) |
| Output | tend_qi_mig | tendency of cloud ice MMR | kg/(kg·s) |
| Output | tend_qr_mig | tendency of rain MMR | kg/(kg·s) |
| Output | tend_qs_mig | tendency of snow MMR | kg/(kg·s) |
| Output | tend_qg_mig | tendency of graupel MMR | kg/(kg·s) |

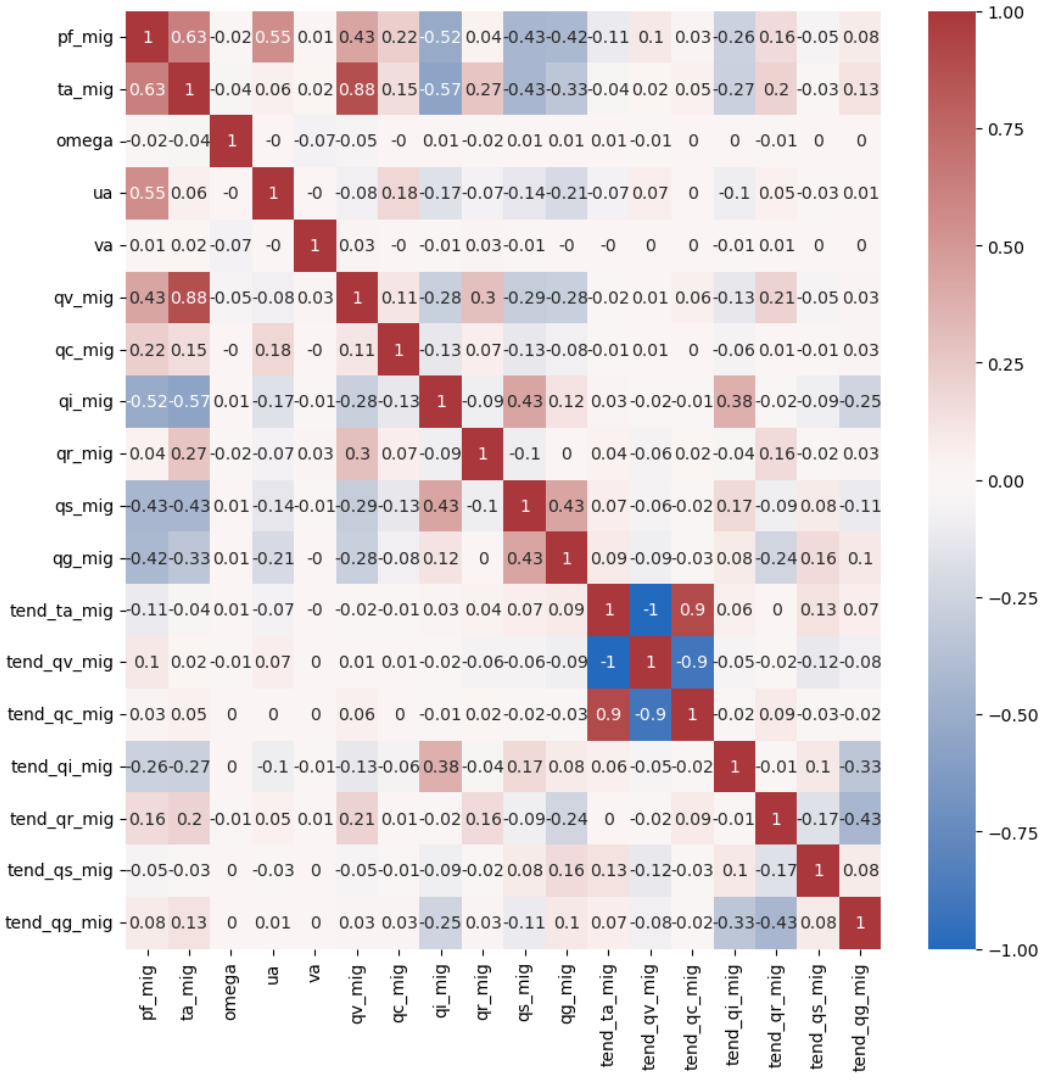


Figure 4: Pearson autocorrelation matrix for all raw input and output parameters. For an explanation of the variable short names, the reader is referred to Table 2. The color bar ranges from negative correlation (blue) over no correlation (white) to positive correlation (red).

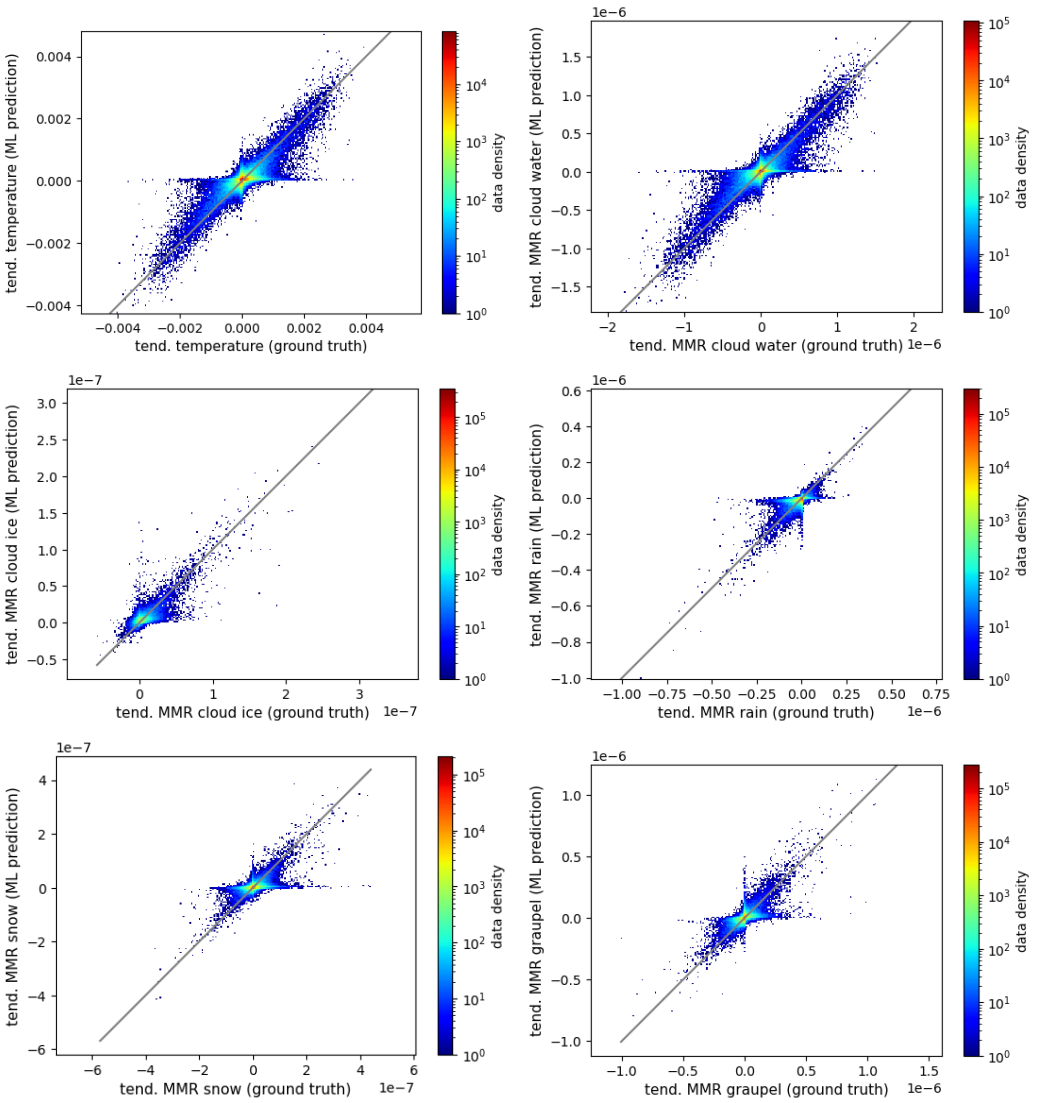


Figure 5: ML predictions vs. ground truth of the additional input variables (for the physics-informed MLP with feature engineering). The colors illustrate the density of the data on a logarithmic scale.